Journal of Geophysical Research: Oceans

RESEARCH ARTICLE
10.1029/2018JC013754

The Weakly Stratified Bottom Boundary Layer of the Global Ocean

D. Banyte[1], D. A. Smeed[2], and M. Morales Maqueda[1]

[1]School of Marine Science and Technology, Newcastle University, Newcastle, UK, [2]National Oceanography Centre, Southampton, UK

Key Points:
- Properties of the weakly stratified bottom boundary layer (wsBBL) are mapped
- The density γ_{wsBBL} and pressure P_{wsBBL} at the upper boundary of the wsBBL are highly correlated
- The γ_{wsBBL}–P_{wsBBL} relation is used to differentiate global ocean subbasins and locations of intensive water transformation

Correspondence to:
D. Banyte,
donata.banyte@newcastle.ac.uk

Citation:
Banyte, D., Smeed, D. A., & Morales Maqueda, M. (2018). The weakly stratified bottom boundary layer of the global ocean. *Journal of Geophysical Research: Oceans*, *123*. https://doi.org/10.1029/2018JC013754

Received 4 JAN 2018
Accepted 30 APR 2018
Accepted article online 11 MAY 2018

Abstract The weakly stratified bottom boundary layer (wsBBL) of the global ocean is currently unmapped; even the definition of the wsBBL layer is yet lacking. However, recent studies point to the wsBBL as a region where most of the abyssal water transformation takes place. In this study, historical high-resolution density profiles are used to map the properties of the wsBBL in the global ocean. We use a density gradient criteria (1×10^{-5} kg m– 4) to define the top of the layer. The thickness of the wsBBL varies from several meters to over a thousand meters and can be used as a rule of thumb to differentiate basin walls from the basin bottom, respectively. Although the thickness varies greatly, the pressure at the top of the wsBBL varies relatively smoothly allowing us to map its distribution across the ocean along with the density of the wsBBL. The neutral density, γ_{wsBBL}, and pressure, P_{wsBBL}, of the upper boundary of the wsBBL are highly correlated within each ocean basin. Diagrams of γ_{wsBBL} versus P_{wsBBL} clearly differentiate the different basins, connected by the narrow channels, along the pathways of abyssal water circulation. The diagrams give insight into the different mechanisms of abyssal water transformation and highlight locations where transformation happens: inter-basin channels and over some parts of mid-oceanic ridges such as found in the Brazil Basin, in the Guiana Basin, and in the Southwest Pacific Basin.

1. Introduction

The deep branch of the meridional overturning circulation (MOC) plays a central role in the uptake of heat and greenhouse gases by the ocean. An understanding of abyssal overturning is therefore important for long-term climate predicitons. The large majority of bottom waters originate in the Southern Ocean and are usually referred to as Antarctic Bottom Waters (AABW). It is widely accepted that AABW are upwelled by diabatic processes, but how and where the abyssal waters become lighter is still debated.

The idea of diapycnal water upwelling being concentrated at the bottom boundary layer (BBL) was recently revived with new theoretical and modelling studies by Ferrari et al. (2016); de Lavergne et al. (2016); McDougall and Ferrari (2017). These studies are founded on the observation that the horizontal area of lighter density surfaces increases with decreasing density because of the concavity of the ocean basins. When density layers intercept the bottom, the BBL fvorms. Within the BBL, turbulent buoyancy fluxes vanish at the solid boundary, creating strong buoyancy flux convergence, hence, diapycnal upwelling. Using idealized simulations, Ferrari et al. (2016) argue that diapycnal upwelling of waters is confined to a thin BBL along the sloping oceanic boundaries and overcomes the diapycnal sinking taking place just above the BBL due to bottom intensified mixing, especially in regions of rough topography (Polzin et al., 1997). Furthermore, weak, but not insignificant, geothermal heatflux further contributes to the lightening of the bottom seawater in the wsBBL. As a result, density layers with the largest bottom intercept area can accumulate large buoyancy fluxes that lead to the strong diabatic upwelling (*de* Lavergne et al., 2016).

Despite its importance in abyssal water transformation, the BBL is currently neither mapped nor well defined. It is recognized that the thickness of the weakly stratified bottom waters vary significantly from one location to the other. Some locations, like the North Pacific Ocean, have notoriously thick layers of weakly stratified abyssal waters, extending over many 100s of meters above the bottom (Mantyla & Reid, 1983), but models often suppose the BBL to be a single vertical bottom grid cell, representing a perception of the BBL being just tens of meters thick.

In this study, properties of the BBL are mapped using hydrographic data from the World Ocean Database (Boyer et al., 2013). Specifically, we investigate the weakly stratified bottom boundary layer (wsBBL)

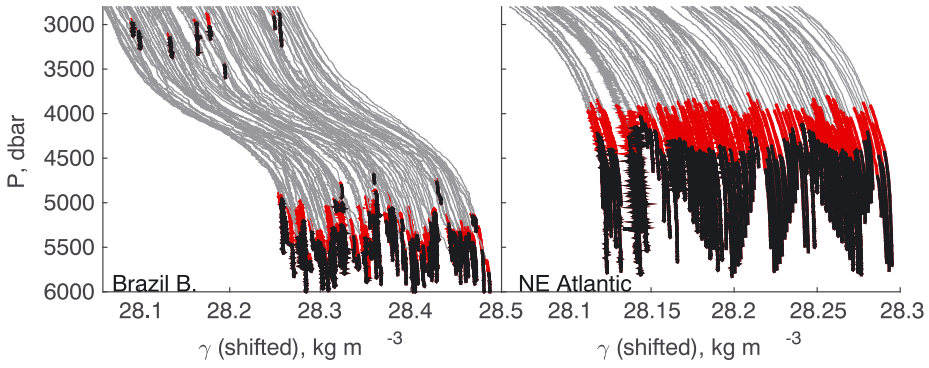

Figure 1. Illustration of the wsBBL search algorithm for the Brazil Basin (left) and the north-east Atlantic basin (right): the density-pressure profiles (gray lines) and their estimated wsBBL using two criteria: a density gradient threshold of 2×10^{-5} kg m^{-4} (upper boundary of red lines), and a density gradient threshold of 1×10^{-5} kg m^{-4} (upper boundary of black lines). The profiles are shifted in density for clarity.

enclosed by the surface below which the density gradient becomes smaller than 1×10^{-5} kg m^{-4}. The results are not sensitive to the precise value of the criteria used. From these data we also map the lateral extents of density layers intercepting the bottom.

We show that neutral density, γ_{wsBBL} (Jackett & McDougall, 1997), and pressure, P_{wsBBL}, of the upper boundary of the wsBBL are highly correlated in global abyssal waters; and both reflect abyssal water circulation pathways. The high coherence of P_{wsBBL} implies that thickness of the wsBBL is, on the contrary, highly dependent on local topography and so more variable. We also show that the $P_{wsBBL} - \gamma_{wsBBL}$ relation can be used to highlight the regions of extreme water transformation: such as narrow inter-basin channels, and several sections of mid-ocean ridges. Finally, we argue that the thickness of the wsBBL serves as a rule of thumb for separating the basin bottom from the sloping basin walls: in the former case the wsBBL is hundreds of meters thick, while in the latter, just meters thick. Incrop areas over basin bottom are shown to be much larger than over the sloping basin walls. These results have important implications for diagnosis of abyssal water transformation.

2. Definition of the wsBBL

For this study, high resolution Conductivity-Temperature-Depth (CTD) profiles deeper than 1,500 m were downloaded from the World Ocean Database (Boyer et al., 2013). A density gradient threshold was used to identify the top of the wsBBL for each profile. Using a gradient criteria has the advantage that it is not affected if a profile does not continue all the way to the sea floor as would be a criteria based on density change. Gradients were evaluated over 100 m intervals and a criteria of 1×10^{-5} kg m^{-4} was used. The density change over 100 m (1×10^{-3} kg m^{-3}) is significantly larger than the accuracy of the CTD measurements of density and the minimum boundary layer thickness that can be resolved is 50 m.

The algorithm for the identification of the wsBBL is illustrated with two sets of example profiles (Figure 1). One set is from the Brazil Basin, with relatively strong abyssal stratification. The other set is from the north-eastern Atlantic, where abyssal stratification is relatively weak. In these examples the density change from the bottom to the estimated top of the wsBBL is of the order of 0.002 kg m^{-3} to 0.003 kg m^{-3} (Figure 1). To quantify the bottom intercept areas of density layers, which following de Lavergne et al. (2016) we refer to hereafter as incrops, a density step that is small compared to the range of bottom densities is required. Typically a density step of 0.005 kg m^{-3} is used. Hence, the examples suggest that the density gradient threshold of 1×10^{-5} kg m^{-4} is small enough to accurately represent finely discretized abyssal density layers at their intercept with the bottom. The wsBBL finding algorithm is described in detail in Appendix A.

Global maps of P_{wsBBL} and γ_{wsBBL} were created by interpolating data from the profile locations using DIVA (Data-Interpolating Variational Analysis) software (Troupin et al., 2012). As the vertical density change within the wsBBL is small, γ_{wsBBL} (Figure 2) is a good approximation to the density of bottom waters. (Mantyla & Reid,

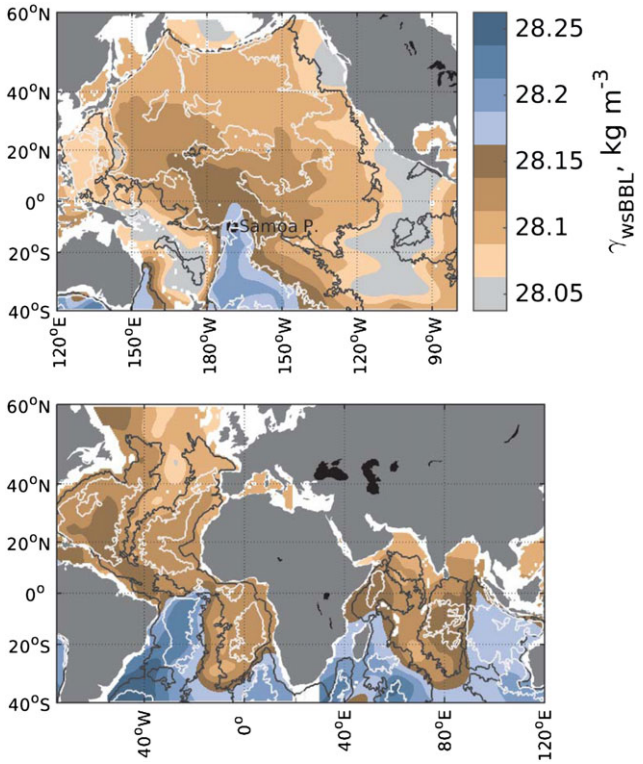

Figure 2. Spatially interpolated density at the upper boundary of the estimated wsBBL (γ_{wsBBL}) using DIVA software (Troupin et al., 2012) not taking into account the local topography. Dark grey contours represent $Z = 4{,}000$ m isobars, while white contours represent $Z = 5{,}000$ m isobars.

1983) showed how the distribution of bottom densities can be used to infer the pathways of bottom waters as they are transformed to lighter densities. Most ocean basins are delineated by their distinctive range of bottom densities. For example, the Samoa Passage, a well documented bottleneck of AABW (Roemmich et al., 1996; Voet et al., 2015), separates the Southwest Pacific Basin and the Central Pacific Basin with a step like change in bottom density.

The P_{wsBBL} map (Figure 3) is less straight forward to interpret. However, areas of deeper P_{wsBBL} are often found downstream of inter-basin connections. This is related to the downward displacement of isopycnals that is a characteristic of flow through topographic choke points (Whitehead, 1998). A notable example is the Vema Channel at the entrance to the Brazil Basin. An especially large area of deep P_{wsBBL} is found in the Northwest Pacific Basin downstream from the Central Pacific Basin. We argue that such deepening of P_{wsBBL} is associated with the two-way exchange of deep waters. This channel serves as a main passage for AABW waters to cross into the northern Pacific, but also as a main passage for lighter Pacific Deep Waters to flow southward above the bottom waters (Kawabe & Fujio, 2010). A similar situation is observed in the Brazil Basin, where both AABW and the North Atlantic Deep Waters (NADW) pass the narrow subbasin, resulting in exceptionally deep P_{wsBBL}. Hence, in both of these examples, the deepening of P_{wsBBL} through the passage is a signature of the two-way exchange of deep and bottom waters. Further insight into the pathways of abyssal waters is provided by considering P_{wsBBL} and γ_{wsBBL} together.

3. The $P_{wsBBL} - \gamma_{wsBBL}$ Relation

In Figures 4–6, we present scatter plots of γ_{wsBBL} versus P_{wsBBL} in the Atlantic, Pacific and Indian Oceans. The figures show that the pressure (P_{wsBBL}) and density (γ_{wsBBL}) at the top of the wsBBL are highly correlated in each of the ocean basins. The upper boundary of lighter incrops are seen to be mostly shallower than denser incrops in the same basin. Furthermore, a progression is seen as bottom waters pass from one basin to the next with the $P_{wsBBL} - \gamma_{wsBBL}$ relation shifting to lighter densities.

In the Atlantic Ocean (Figure 4), P_{wsBBL} and γ_{wsBBL} are highly correlated in each of the subbasins, with a few important exceptions discussed below. The densest water north of 40°S is found in the Argentine Basin and in the Cape Basin. These two basins are separated by the Mid-Atlantic Ridge (MAR). Abyssal flow northward from the Cape Basin is completely blocked by the Walvis Ridge and the only source of AABW in the rest of the Atlantic ocean is from the Argentine Basin. As the AABW passes the Vema channel into the Brazil Basin there is a reduction in bottom density and a deepening of P_{wsBBL}. There is then an even greater discontinuity in bottom densities between the Brazil Basin and the North West Atlantic subbasin. In contrast, the $P_{wsBBL} - \gamma_{wsBBL}$ relation for the north and south basins of the eastern Atlantic almost overlap and there is little distinction between them.

There are two large areas where the $P_{wsBBL} - \gamma_{wsBBL}$ relation is found to be significantly different from the surrounding basins: the flanks of the Mid-Atlantic Ridge in the Brazil Basin and in the tropical north-western Atlantic basin southward of 20°N. In the former region, the wsBBL is significantly lighter than elsewhere in the Brazil Basin and its $P_{wsBBL} - \gamma_{wsBBL}$ relation is significantly steeper than in the rest of the Brazil Basin. This region is well documented as location of intense abyssal mixing and extreme water transformation (Ledwell et al., 2000; Polzin et al., 1997). In the north-western Atlantic basin, the region of anomalous $P_{wsBBL} - \gamma_{wsBBL}$, being at the entrance to the basin, has the densest abyssal waters in the basin. However, similar to the MAR in the Brazil Basin, waters undergo a rapid transformation in a short distance. The data in Figure 4 suggests that both of these anomalous regions contribute to the large density change (0.1 kg m^{-3}) between the Brazil and north-western basins. No such hotspots of mixing are evident in the eastern Atlantic.

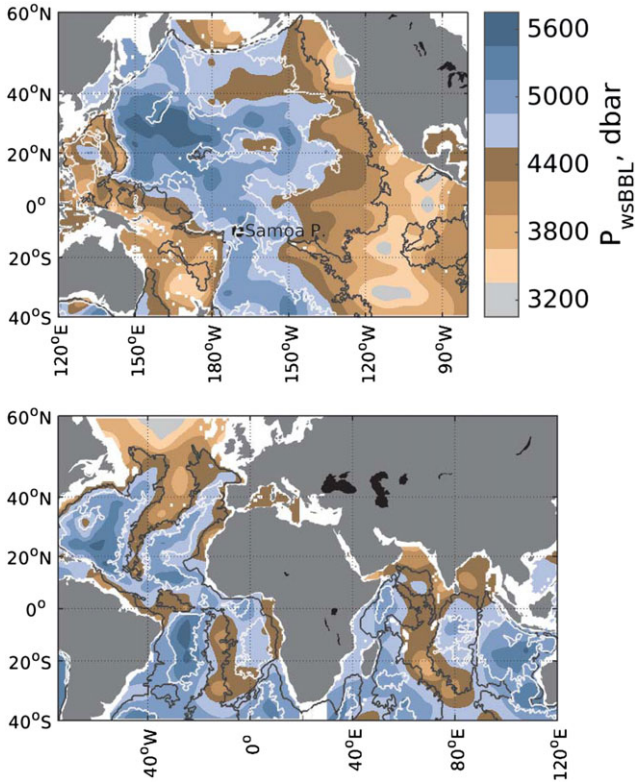

Figure 3. Same as Figure 2, but for the upper boundary of the estimated wsBBL (P_{wsBBL}).

In the Pacific Ocean (Figure 5), there are four major subbasins: the Southwest Pacific, the Central Pacific, the North Pacific, and the Tropical Eastern Pacific. The Southwest Pacific Basin has similar characteristics to the Brazil Basin in the Atlantic Ocean, though the bottom waters in the Southwest Pacific Basin are significantly lighter and their estimated P_{wsBBL} are significantly shallower. This subbasin is located to the west of the East Pacific Rise (EPR), a fast spreading ridge analogous to the mid-Atlantic Ridge. Over the EPR, the $P_{wsBBL} - \gamma_{wsBBL}$ relation is very different from that in the rest of the basin. Similar to the western flank of MAR, much lighter densities incrop here; their P_{wsBBL}, though shallower, are deeper than would be expected from the $P_{wsBBL} - \gamma_{wsBBL}$ relation for the rest of the basin. This too is a hotspot of abyssal water transformation for a large density range of abyssal waters.

From the Southwest Pacific Basin, abyssal waters spread to the Central Pacific Basin through the Samoa Passage. The flow through the passage is hydraulically controlled and the site of intense turbulence resulting in the entrainment of lighter waters into the BBL (Alford et al., 2013; Freeland, 2001). The density change across the Samoa passage is about 0.025 kg m^{-3} and is accompanied by a significant deepening of P_{wsBBL}. Within the Central Pacific Basin a similar reduction in density is also observed, and P_{wsBBL} and γ_{wsBBL} are poorly correlated suggesting significant amounts of mixing within this basin.

From the Central Pacific Basin, the northward spread of abyssal waters branches westward and eastward (e.g., Roussenov et al., 2004). For the western branch, the $P_{wsBBL} - \gamma_{wsBBL}$ relation highlights the transition zone (violet dots in Figures 5) into the North Pacific subbasin, which is the largest subbasin in the global ocean. For the eastern branch, no such clear transition zone is identified with our data. However, the $P_{wsBBL} - \gamma_{wsBBL}$ relation, by shifting to lighter densities, indicates an eastern abyssal flow pathway from the Central Pacific Basin to the Tropical Eastern Pacific subbasin, and finally to the Northern Pacific subbasin, in agreement with modeling studies (Roussenov et al., 2004) and observations (Kawabe & Fujio, 2010).

Finally, the Philippine Basin has the lightest bottom waters in the Pacific. These consist of diluted Pacific Deep Water that has passed through the gaps in the East Mariana and Yap ridges (Chaen et al., 1993; Gamo, 1993). The Philippine Basin is an example of many small semi-enclosed subbasins found in the global ocean where P_{wsBBL} and γ_{wsBBL} properties are highly correlated for bottom waters with different water mass characteristics.

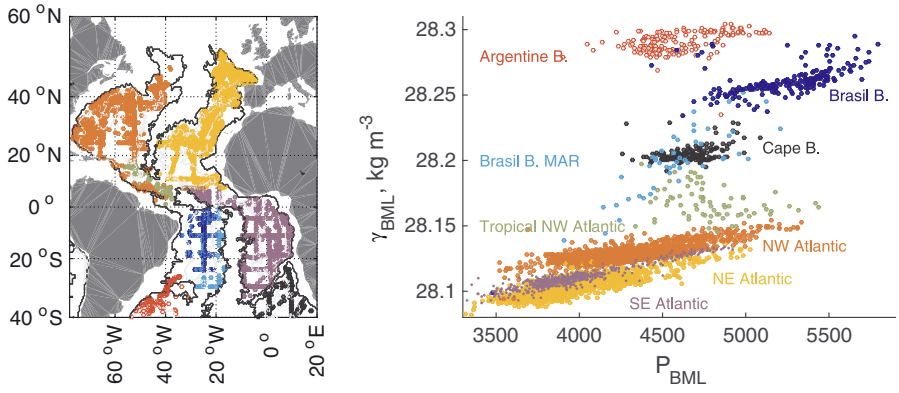

Figure 4. $P_{wsBBL} - \gamma_{wsBBL}$ relation for different subbasins in the Atlantic Ocean: the Argentine Basin (empty red circles), the Brazil Basin (dark blue circles), the MAR region in the Brazil Basin (light blue circles), the North West Atlantic subbasin (full red circles), its tropical part (green circles), the North East Atlantic subbasin (orange circles), the South East Atlantic subbasin (violet circles), the Cape Basin (black circles).

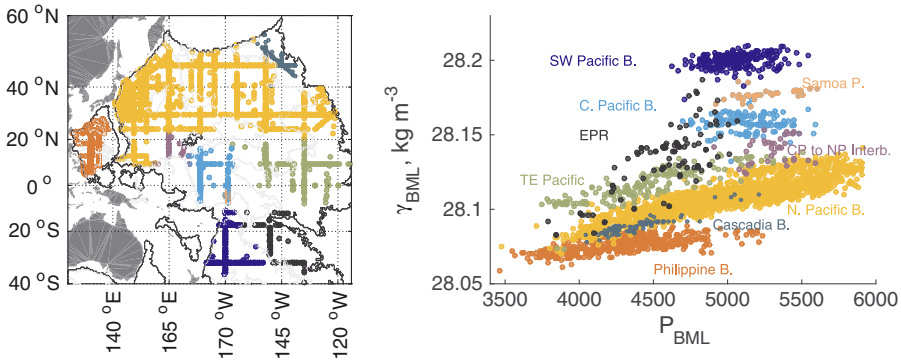

Figure 5. $P_{wsBBL} - \gamma_{wsBBL}$ relation for different regions in the Pacific Ocean: the Southwest Pacific Basin (SW Pacific B.), its region on the flanks of the EPR, downstream the Samoa passage region, the Central Pacific Basin (C. Pacific B.), the interbasin passage between the Central Pacific Basin and North Pacific subbasin (CP to NP Interb.), the North Pacific subbasin (N. Pacific B.), the Tropical Eastern Pacific subbasin (TE Pacific), and the Philippine Basin.

The Indian Ocean has two northward routes for abyssal waters: the eastern and western branches, separated by the Central Indian Ridge and South East Indian Ridge (Mantyla & Reid, 1995). Due to a lack of data, we clustered the data from several subbasins mainly to illustrate the strong $P_{wsBBL} - \gamma_{wsBBL}$ relation for the far-end subbasins of AABW circulation pathway. The western branch of abyssal flow encounters a large number of confined basins: Crozet, Madagascar, Mascarene, Somali, with the largest and far-end subbasin being the Arabian Basin. Along the eastern pathway, the northward spreading abyssal waters fill the basins: South Australia, Perth, West Australia, until reaching its largest far-end subbasin - the Central Indian Basin.

The two end basins, the Arabian Basin and the Central Indian Basin, are both relatively well sampled and each has tight correlation between P_{wsBBL} and γ_{wsBBL} (Figure 6), but in the Arabian Basin densities are much lighter. This is despite the fact that AABW entering the western branch is significantly denser than that entering the eastern branch. The larger change in density on the western branch suggests the existence of a number of mixing hotspots on the western side of the Indian Ocean, in agreement with observed asymmetry in the rate of tidal energy dissipation (Egbert & Ray, 2000) and the greater number of constricting passages along the northward pathway of abyssal waters.

4. Incrop Areas Inside Subbasins

The abyssal waters originating southward of 40°S latitude spread northward by filling basin after basin. As shown above, the $P_{wsBBL} - \gamma_{wsBBL}$ relation can be used to differentiate the sequence of basins. Each subsequent subbasin is filled with progressively lighter waters and within the basin, lighter waters are associated with the shallower P_{wsBBL}. In this section we show that in each basin, lighter density incrops are associated

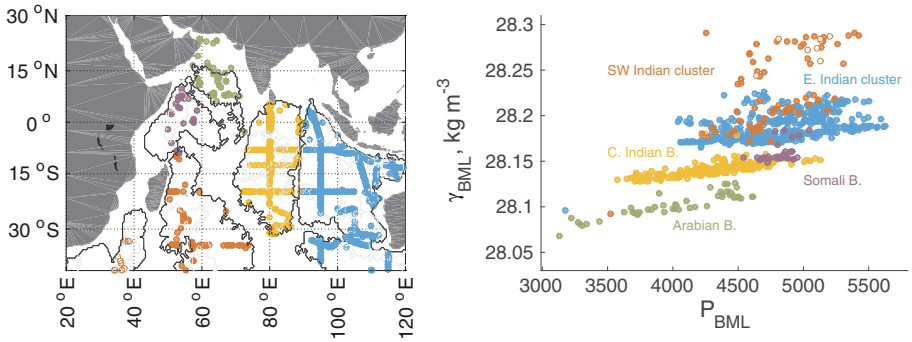

Figure 6. $P_{wsBBL} - \gamma_{wsBBL}$ relation for different subbasins in the Indian Ocean: the Mozambique Basin (empty red circles), the clustered Crozet, Madagascar, and Mascarene basins (red circles), the Somali Basin (violet circles), the Arabian Basin (green circles), the clustered Perth, Wharton, Cocos, North Australia basins (blue circles), the Central Indian Basin (orange circles).

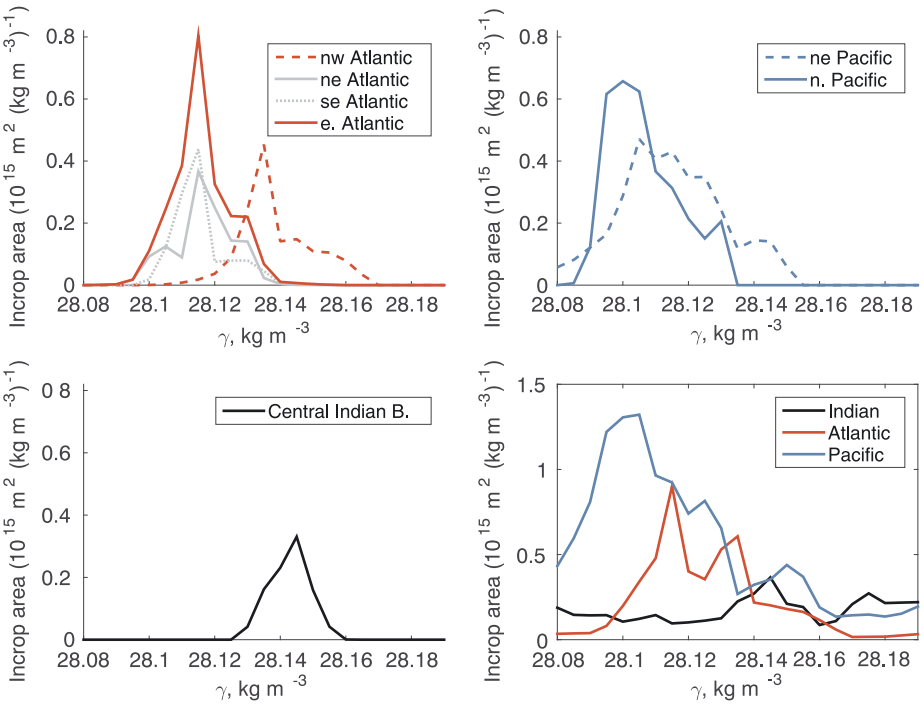

Figure 7. Size of incrop areas for discretized density layers in the Atlantic subbasins (top left): the North West Atlantic subbasin (nw Atlantic), the North East Atlantic subbasin (ne Atlantic), the South East Atlantic subbasin (se Atlantic), and the whole East Atlantic (e. Atlantic), in the Pacific subbasins (top right): the Tropical Eastern Pacific subbasin (ne Pacific), the North Pacific subbasin (n. Pacific), in the Central Indian Basin (bottom left), and for the whole three oceans north of 40°S (bottom right). Incrop area estimates take into account the local topography, omitting too shallow regions.

with larger incrop areas, and, the far-end basins, hosting the lightest bottom waters, have the largest incrop areas of all.

In the Atlantic ocean, abyssal waters advance from the Brazil Basin branch to the north-western as well as to the eastern Atlantic subbasins. In the North West Atlantic subbasin, the largest incrop area is found for the density layer of γ=28.13±0.0025 kg m^{-3} (Figure 7), which is one of the lightest abyssal waters in this basin and and is found in the western and northern parts (Figure 8). The eastern Atlantic is filled with even lighter waters suggesting the whole eastern Atlantic to be the end subbasin of the AABW spreading in the Atlantic Ocean. The largest incrop area is found for the density layer of 28.11 ±0.0025 kg m^{-3} which fills most of the Angola Basin. This explains the exceptionally weak abyssal stratification in the Angola Basin (Thurnherr & Speer, 2003). Although it is in the Southern Hemisphere, the Angola Basin is in some ways analogous to the North Pacific ocean being the end of the abyssal circulation of the AABW.

In the Pacific ocean, the $P_{wsBBL} - \gamma_{wsBBL}$ relation identifies the region north of 20°N as the far-end subbasin of abyssal circulation. Here, the largest incrop area is associated with the density layer γ=28.100±0.0025 kg m^{-3} (Figure 7) that spreads through the central and eastern parts of the subbasin (Figure 8). The second largest subbasin in the Pacific ocean is the Tropical Eastern Pacific subbasin. Its largest incrop area is associated with slightly denser water, γ=28.105±0.0025 kg m^{-3}, and the area is approximately 30% smaller than the largest incrop area in the North Pacific subbasin.

Globally, the far-end subbasin of the Pacific Ocean is filled with the lightest bottom waters, which have the largest incrop areas. The incrop areas in the Atlantic Ocean are significantly smaller. However, Atlantic Ocean has a characteristic two peak distribution of the incrop area versus density profile (Figure 7); one is associated with the north-west Atlantic and the other with the eastern Atlantic. Bottom waters of the eastern Atlantic are strongly diluted with the North Atlantic Deep Waters (Johnson, 2008). Hence, the NADW becomes increasingly in contact with the bottom in the eastern Atlantic. We argue below that two peak distribution in the size of incrop areas is a result of two bottom water sources. Finally, the Indian Ocean has the smallest incrop areas the largest of which is associated with the density layer 28.145 ±0.0025 kg m^{-3}, located over

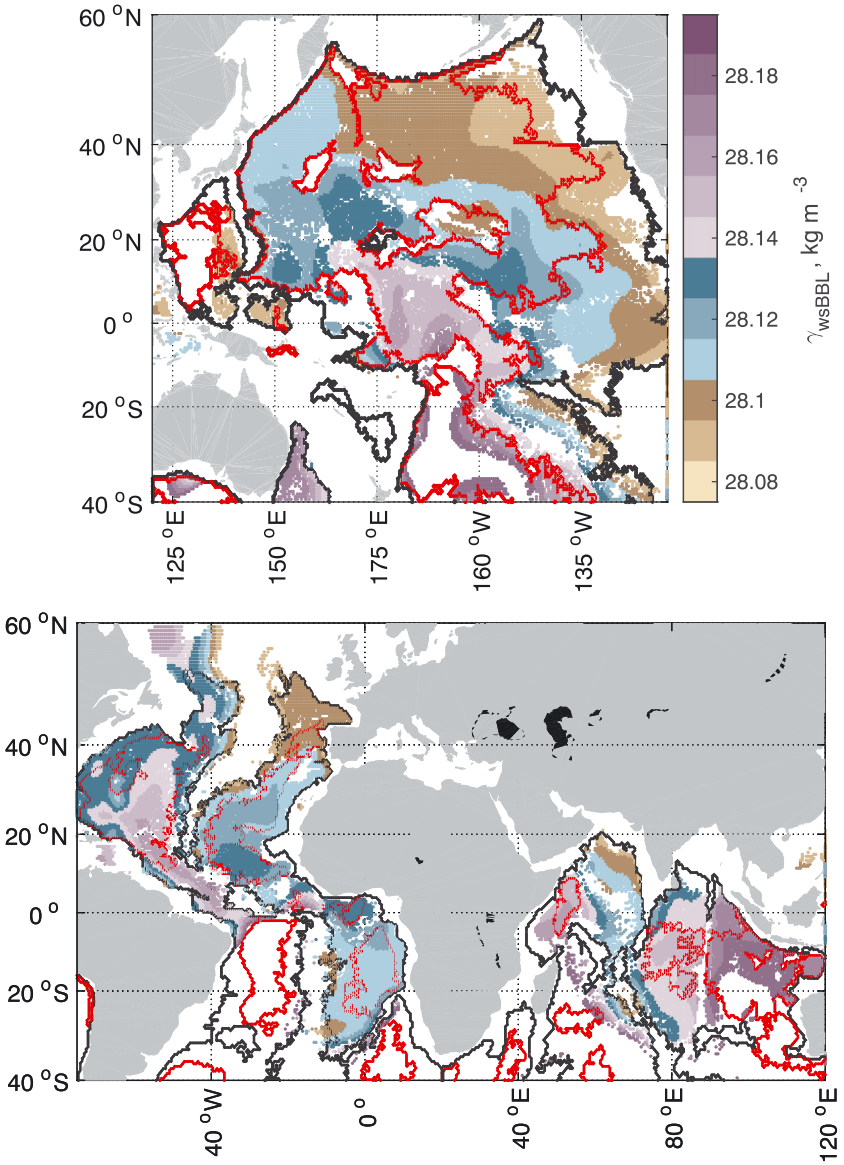

Figure 8. Figure 8.Map of the incrops for a lighter range of abyssal waters discretized with 0.01 kg m^{-3} density step. Black contours represent $Z = 4{,}000$ m isobars, while red contours represent $Z = 5{,}000$ m isobars.

the Central Indian Basin: the far-end subbasin of the eastern branch of abyssal water circulation. In conclusion, throughout the global ocean, the lighter density layers tend to have larger incrop areas with the largest incrops located in the far-end subbasins of the AABW pathways.

5. Thickness of the wsBBL

The strong correlation of P_{wsBBL} and γ_{wsBBL} and their smooth variation within basins enables spatial interpolation of these variables in the sparsely sampled abyssal ocean. In contrast, the depth of the wsBBL depends on the local topography and is much more variable. The thickness of the wsBBL is calculated as the difference of the interpolated values of P_{wsBBL} and the bathymetry (Figure 9). It can be seen that far-end subbasins with the lightest bottom waters also tend to have the thickest wsBBL layer. There are large regions where the wsBBL thickness exceeds 1,000 m, these are spread throughout the north Pacific ocean, and the eastern Atlantic, especially in the Angola Basin (Figure 9). The precise thickness of the wsBBL depends upon the value chosen for the density gradient criteria but the pattern of variability is not dependent upon the value used.

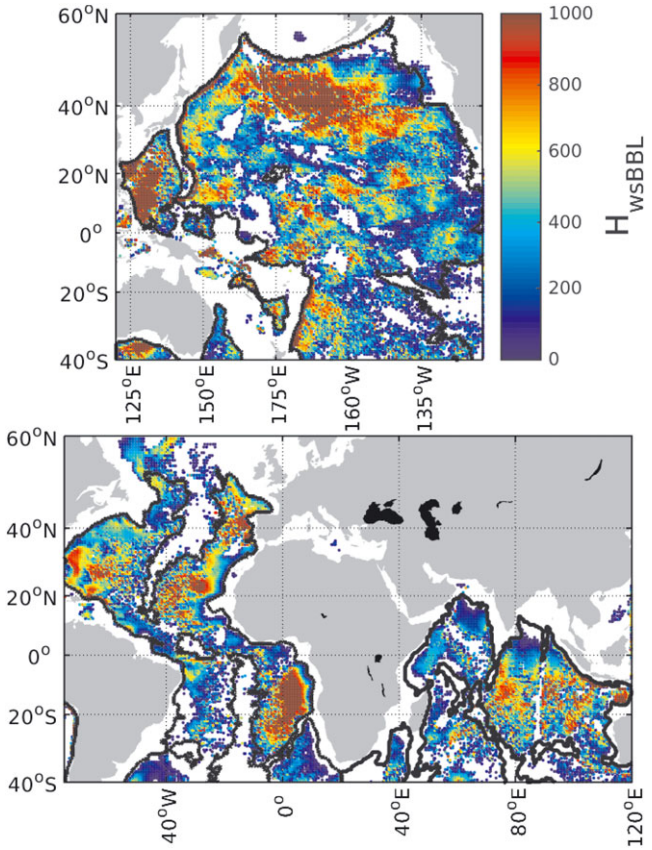

Figure 9. Thickness of wsBBL (H^i_{wsBBL}) estimated as a residual of Z^i-P^i_{wsBBL}, where i marks a spatial location, Z^i is the water column height and P^i_{wsBBL} is an upper boundary of the estimated wsBBL at that location.

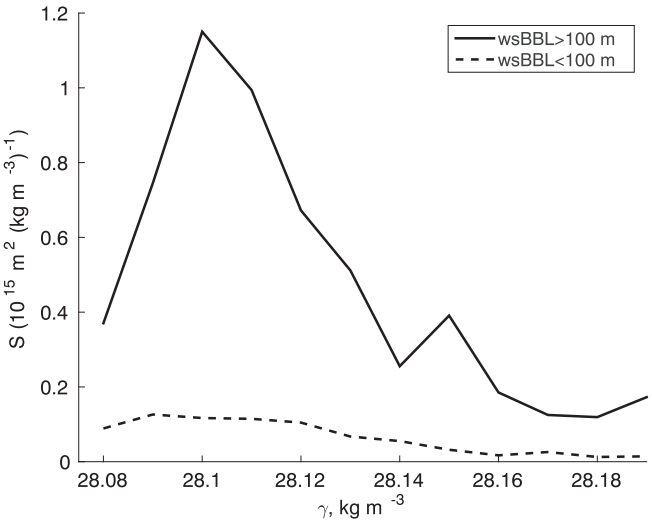

Figure 10. Bottom intercept areas estimated for the Pacific Ocean for the density layers with 0.01 kg m^{-3} resolution, where the wsBBL is projected to be thicker than 100 m (solid line) and thinner than 100 m (dashed line).

The wsBBL thickness map allows exploration of the regions where density layers are in close proximity to the basin boundaries, e.g., where thickness of the wsBBL drops below 100 m. Only small parts of the largest incrops have wsBBL smaller than 100 m. In the Pacific Ocean, only 10% of the largest incrop, associated with the density layer γ_{wsBBL}=28.10±0.005 kg m^{-3}, has such thin wsBBL (Figure 10) and these areas closely follow the contours of ridges and coasts - the walls of the basin.

6. Conceptual Model of Incrops

Here, we discuss a simple conceptual model as was used by de Lavergne et al. (2017) to estimate global abyssal water upwelling (S1 scenario in de Lavergne et al., 2017). The model assumes uniform local density fluxes both by turbulent mixing and geothermal heating over a series of interconnected basins, each of which have sloping walls. We show that this simple model can explain several observed features of the wsBBL: 1) the increase in incrop areas with lighter waters, 2) the largest incrop areas being found in the far-end subbasins, 3) the two orders of magnitude variation in the thickness of the wsBBL.

In contrast to the previous studies of Ferrari et al. (2016); McDougall and Ferrari (2017); de Lavergne et al. (2017), we consider each subbasin to be a broad channel like basin rather than a cone shaped basin. Application of the water transformation framework of Walin (1982) states that the conservation of volume in a steady state is a balance between the total inflow of abyssal waters of densities smaller than γ ($\Phi(\gamma)$) and the diapycnal upwelling ($G(\gamma)$) through the density layer γ: $\Phi(\gamma)=G(\gamma)$. Assuming that diffusive buoyancy flux as well as geothermal heating are uniform, the water mass transformation happens at the bottom boundary, where buoyancy fluxes converge. In this case, the water mass transformation is proportional to the incrop area ($A(\gamma)$), which is a bottom intercept area per unit of density: $A(\gamma)=\partial S/\partial\gamma$, where $S(\gamma)$ is the horizontal area covered by isopycnals of density equal or larger than γ. As a result, large incrop areas can accumulate large buoyancy fluxes, both geothermal and diffusive. The mass and volume balance must be valid for any abyssal density layer. Hence, for density layers $\gamma_1 > \gamma_2 > \ldots > \gamma_T$ the following relations hold: $\Phi_1<\Phi_2<\ldots<\Phi_T$ and $G_1<G_2<\ldots<G_T$, which can be achieved with $A_1<A_2<\ldots<A_T$. It follows that the lightest abyssal water layers have the largest incrop areas.

Assuming that, away from the boundary, density layers are almost flat, then at their incrop the lightest densities extend higher up in the water column, and so a thicker layer of weak stratification ensues (Figure 11). As a result, abyssal stratification is largest at the source-end of the basin, where wsBBLs are thin and the incrop areas are small. At the far-end, on the contrary, the abyssal stratification is weak and the incrops become very large and very thick. If the channel length is limited, the incrop areas cannot increase indefinitely and the bottom of the ocean is filled. The density layer with the largest incrop area becomes the upper boundary of the abyssal water layer. The dense water that forms at the far-end of the basin then is the lower boundary of the water layer out-flowing from the basin.

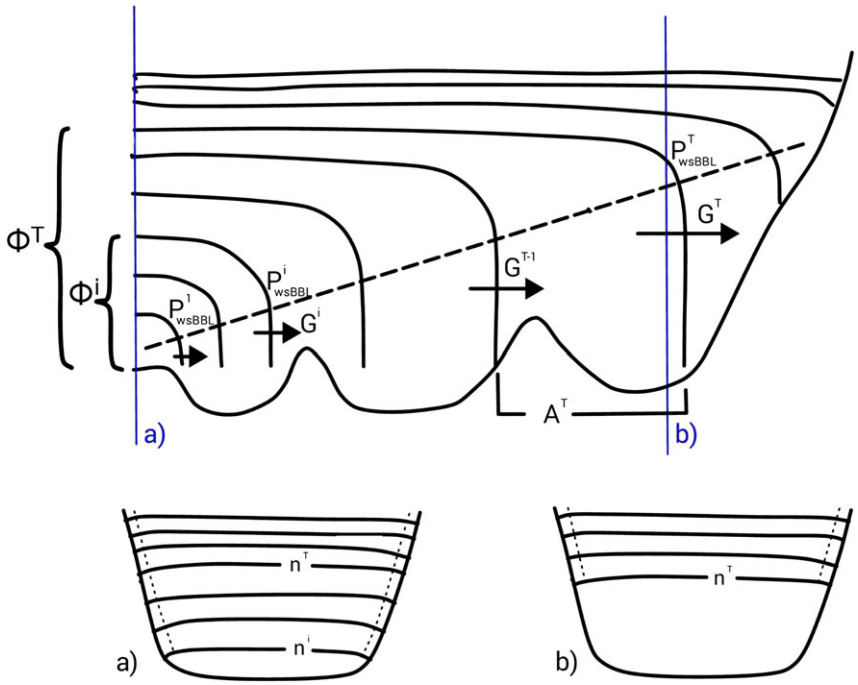

Figure 11. Schematics of discretized density layers and their incrops in a single channel-like subbasin with sloping basin walls: meridional transect (above), zonal transect at the source-end (a), and zonal transect at the far-end (b). Φ^i marks the integral abyssal water flow into the subbasin enveloped by the density layer n^i, G - integral abyssal water transformation through the density layer n^i, A^T marks the largest bottom intercept area of the density layer enveloped by density surfaces n^{T-1} and n^T, while thick dashed line marks the depth of the upper boundary of the wsBBL (P_{wsBBL}).

This study shows that oceanic basins can be modeled as a series of interconnected subbasins, where mixing in the passages leaves a clear mark on both incrop properties: density (γ_{wsBBL}) and pressure (P_{wsBBL}). In a single subbasin, P_{wsBBL} becomes shallower with lighter incrop densities. However, after passing into the next subbasin, both deepening of the density surfaces and almost step-like reduction in bottom density is commonly observed. Thus, the connectig passages act as hotspots of turbulent mixing and abyssal water transformation. However, when away from such mixing hotspots, the strength of abyssal water transformation is once again defined largely by the incrop areas.

If local diffusive buoyancy fluxes or geothermal heating are the same in the subsequent subbasin, the incrops become larger than in the first subbasin to account for the larger integral water influx and diapycnal water upwelling, the same as for a single subbasin (Figure 12). As incrop areas increase with each subsequent subbasin, the subbasin size also tends to increase. This is achieved by a shallower P_{wsBBL} with lighter density incrops. As a result, the end-flow abyssal subbasins are the largest, their incrops have the shallowest P_{wsBBL} and large regions where weak abyssal stratification is very thick. As ocean size is limited, only a small number of subbasins are possible, until the bottom of each ocean is filled with the abyssal waters.

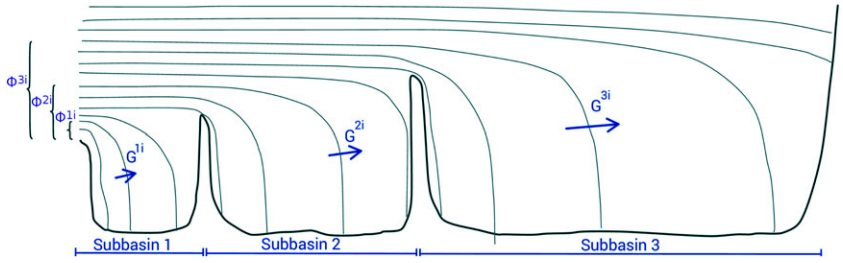

Figure 12. Same as in Figure 11, but for the discretized density layers and their incrops along the series of subbasins.

If two water masses of different origin mix, as is the case for AABW and NADW in the Atlantic, the lighter waters (NADW) eventually gain access to the bottom, and the simple relation between incrop area and bottom density breaks. While such scenario needs further exploration, we anticipate that the two peak distribution seen in Figure 7 for the Atlantic is caused by the high percentage of NADW found in the bottom waters of the Eastern Atlantic.

Finally, in the real ocean, neither turbulent buoyancy fluxes nor geothermal heating are uniform in space, but the increase in the incrop areas for lighter abyssal water layers is globally observed (de Lavergne et al., 2016). They conclude that 1) abyssal water transformation happens mostly at the bottom boundary, 2) the lightest abyssal waters have the largest incrop area, and 3) diapycnal upwelling is largest for the lightest abyssal waters with the largest incrop area.

7. Discussion

We have shown that the $P_{wsBBL} - \gamma_{wsBBL}$ relation can be used as a tool to differentiate the topographically enclosed subbasins through which abyssal waters pass when filling the bottom of the oceans. From one subbasin to the next, the $P_{wsBBL} - \gamma_{wsBBL}$ relation shifts to lighter densities. The same relation highlights the regions of extensive water transformation. The most evident of which are the flanks of mid-oceanic ridges in the Brazil Basin, in the tropical north-western Atlantic, and in the Southwest Pacific Basin. Thus, this study highlights the importance of mixing in straits and passages (Bryden & Nurser, 2003) as well as strong mixing along parts of the mid-ocean ridges in the upwelling of abyssal waters.

Equally important is the use of the P_{wsBBL} and γ_{wsBBL} properties to differentiate the oceanic basin bottom from oceanic basin walls. The interpolated map of P_{wsBBL} together with the topography identifies regions of thin wsBBL (e.g., less than 100 m, in this study), which are associated with the oceanic basin walls. We show that such areas contribute only little to the size of the largest incrops.

The differentiation of oceanic basin bottom from its walls is a novel concept that can not be explained using the visualization of ocean as a cone-shape vessel. Such visualization laid the foundation for the hypothesis of the diabatic water upwelling at the bottom boundary of the basin (de Lavergne et al., 2016, 2017; Ferrari et al., 2016; McDougall & Ferrari, 2017). The cone-shaped ocean well visualizes the increase in the surface area of lighter neutral density surfaces through the bottom intercept areas. This can cause the density flux divergence, or diabatic water upwelling, even at the presence of the bottom intensified mixing near the sloping walls of the basin (Ferrari et al., 2016; Klocker & McDougall, 2010). However, in the cone-shaped basin, the incrops are defined as density layer intercepts with the sloping walls, where just meters thick wsBBL forms, supported by observations over the continental shelves (e.g., Moum et al., 2004).

Instead, we show here that wsBBL can vary two orders of magnitude, which can be explained with the conceptual model of abyssal waters in a broad channel-like basin. Such conceptual models are used to investigate the meridional spread of AABW from the southern source (Ferrari et al., 2016; Mashayek et al., 2015). Interestingly, Ferrari et al. (2016) used a model with a channel-like oceanic basin to investigate abyssal water upwelling along the sloping basin boundaries, but interpreted the results by using a cone-shaped oceanic visualization. As a result, they argued that the basin with perpendicular walls (their Box-MixBottom simulation) and realistic turbulent density fluxes produce abyssal stratification not consistent with the observations: exceptionally weak at the far-end of the basin. Here, we confirm that in the real ocean the far-end subbasins have exceptionally weak stratification with wsBBL over a thousand of meters thick. Hence, we argue that their simulation of the basin with perpendicular walls (Box-MixBottom simulation) might be more realistic than their simulation with sloping basin walls (Bowl-MixBottom simulation). Their modeling simulations confirm that incrop areas can increase even without sloping basin walls.

Finally, the visualization of oceanic basin as cone-shaped also creates an impression of topographic control on the size of incrop areas: an argument explored by the recent study of de Lavergne et al. (2017). They argue that a cumulative function of incrop areas with density is a result of the seafloor distribution with depth. However, the cumulative function of incrop areas with density only reflects the increase in incrop areas of lighter abyssal waters. As incrop areas increase along the bottom of the ocean, not their walls, the similar cumulative function of incrop areas can be obtained by using a simple model of channel-like oceanic basin with flat bottom and perpendicular walls, as well as homogeneous turbulent density fluxes. As a result, the

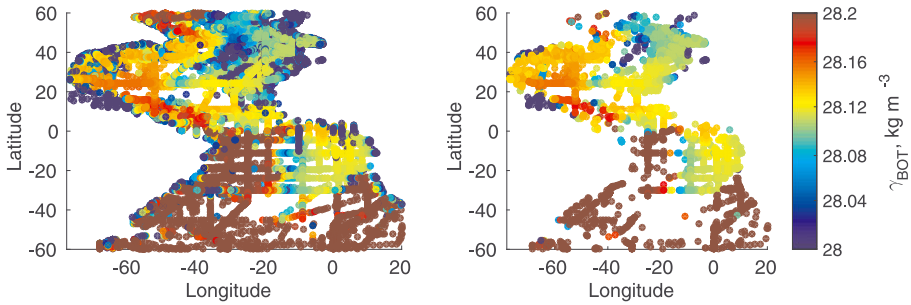

Figure A1. Median density in the deepest 20 m of each profile. For all profiles (left) and only for profiles where the estimated wsBBL is thicker than 100 m (right) in the Atlantic Ocean.

size distribution of incrops is a dynamical property, not set by the topography. Furthermore, the large thickness of wsBBL, especially at the far-end subbasins, substantially reduces the topographic constrains. Not surprisingly, the far-end subbasins are large in size and host the largest bottom intercept areas.

While we suggest the use of the thickness of the wsBBL as a rule of thumb to differentiate oceanic walls from the bottom, we also point to the places where such a rule fails. Here we have shown that large scale hotspots of turbulent mixing, like the flanks of MAR in the Brazil Basin substantially modify the $P_{wsBBL} - \gamma_{wsBBL}$ relation: much lighter densities have incrops with thick wsBBL. In general, light waters are excluded from the bottom; they outcrop at the walls of the basin and result in very thin wsBBL. However, the density surfaces bend when approaching the hotspots of mixing like the MAR of Brazil Basin (Ledwell et al., 2000). As a result, over such locations the boundary between the oceanic basin walls and the bottom start to merge. This observation also calls for caution when extrapolating the high water transformation and turbulent mixing observed over the well investigated mid-ocean ridge of the Brazil Basin to the global scales.

Finally, the fact that the wsBBL is hundreds of metres thick over most of the abyssal ocean suggests that it cannot be assumed that the wsBBL is contained within the deepest grid cell of models when estimating the rates of abyssal water transformation.

Appendix A: Criteria for the wsBBL

For this study, high resolution data of Conductivity-Temperature-Depth (CTD) profiles deeper than 1,500 m were downloaded from the global World Ocean Database (downloaded in October 2016). A density gradient threshold method was used to identify the wsBBL. The density gradient was computed over 100 m intervals with the depth step of 4 m. Both parameters were chosen subjectively, noting that meaningful density gradients have to be computed over a reasonably large depth interval so that they are not affected by spikiness in the data. Intrusions with a density gradient larger than the threshold were allowed if they extended less than 20 m. As a result, the method can not estimate the wsBBL thinner than 50 m: half of the depth interval over which the density gradient is computed. We have only presented results for profiles with a wsBBL thicker than 100m and have excluded all those with shallow wsBBLs (Figure A1).

We tested two density gradient thresholds: $C_1 = 1 \times 10^{-5}$ kg m^{-4} and $C_2 = 2 \times 10^{-5}$ kg m^{-4}. All the results in this study are provided for the wsBBL defined by the criteria C_1, but below we compare with the results obtained with the C_2 criteria and show that the choice does not significantly affect our conclusions. The wsBBL search algorithm is visualized for two locations: in the Brazil Basin and in the north-eastern Atlantic Ocean along 24.5°N transect (Figure 1). The former has strong abyssal density gradients, while the latter is weakly stratified high up in the deep water column. In the Brazil Basin, both criteria (C_1 and C_2) yielded a wsBBL that is deeper than a rapid increase in density gradients observed at approximately 4000 − 4500 m depths, caused by the counter flow of the NADW above the AABW.

The median wsBBL thickness estimated for the profiles in the Brazil Basin is: 200 m (C_1) and 340 m (C_2). The median estimate of the wsBBL upper boundary is: 5,450 m (C_1) and 5,310 m (C_2). In the north-eastern Atlantic with very smooth transition in stratification between the bottom and mid-depth, the wsBBL thickness is: 830 m (C_1) and 1,270 m (C_2), while the wsBBL upper boundary is: 4,460 m (C_1) and 4,020 m (C_2). Abyssal waters in

the north-eastern Atlantic are much more homogeneous. The surface below which the stratification becomes low is located almost 1,000 m higher up in the water column. However, while stricter criteria result in a significantly thinner and deeper wsBBL, both yield the same conclusions on how wsBBL properties relate to the large scale abyssal ocean circulation.

The resulting median density difference over the wsBBL as estimated for the profiles plotted in Figure 1 is: 0.0015 kg m^{-3} (C_1) and 0.0030 kg m^{-3} (C_2) for the Brazil Basin and 0.0030 kg m^{-3} (C_1) and 0.0090 kg m^{-3} (C_2) for the north-eastern Atlantic. Hence, both criteria are small enough to represent the vertical extent of discretized abyssal density layers with a density step of 0.005 kg m^{-3} or 0.01 kg m^{-3}.

Acknowledgments
This research was supported by the NERC OSCAR project grant NE/I022868/1 (M. Morales Maqueda and D. Smeed). The global data were mapped using DIVA (Data-Interpolating Variational Analysis) software. We thank C. de Lavergne for valuable discussions. The data from this campaign are made available through the British Oceanographic Data Centre (bodc.ac.uk).

References

Alford, M. H., Girton, J. B., Voet, G., Carter, G. S., Mickett, J. B., & Klymak, J. M. (2013). Turbulent mixing and hydraulic control of abyssal water in the Samoan Passage. *Geophysical Research Letters*, *40*, 4668–4674. https://doi.org/10.1002/grl.50684

Boyer, T. P., Antonov, J. I., Baranova, O. K., Coleman, C., Garcia, H. E., Grodsky, A., et al. (2013). World Ocean Database 2013. In S. Levitus (Ed.), *NOAA Atlas NESDIS 72*, A. Mishonov (Technical Ed.) (209 pp.). Silver Spring, MD. https://doi.org/10.7289/V5NZ85MT

Bryden, H. L., & Nurser, A. J. (2003). Effects of Strait Mixing on Ocean Stratification. *Journal of Physical Oceanography*, *33*, 1870–1872.

Chaen, M., Fukasawa, M., Maeda, A., Sakurai, M., & Takematsu, M. (1993). Abyssal boundary current along the Northwestern Perimeter of the Philippine Basin. *Elsevier Oceanography*, *59*, 51–67. https://doi.org/10.1016/S0422-9894(08)71317-5

de Lavergne, C., Madec, G., Le Sommer, J., Nurser, A. J. G., & Garabato, A. C. N. (2016). On the consumption of Antarctic bottom water in the abyssal ocean. *Journal of Physical Oceanography*, *46*, 635–661.

de Lavergne, C., Madec, G., Roquet, F., Holmes, R. M., & McDougall, T. J. (2017). Abyssal ocean overturning shaped by seafloor distribution. *Nature*, *551*, 181–186.

Egbert, G. D., & Ray, R. D. (2000). Significant dissipation of tidal energy in the deep ocean inferred from satellite altimeter data. *Nature*, *405*, 775–778.

Ferrari, R., Mashayek, A., McDougall, T. J., Nikurashin, M., & Campin, J. M. (2016). Turning ocean mixing upside down. *Journal of Physical Oceanography*, *46*, 2239–2261. https://doi.org/10.1175/JPO-D-15-0244.1

Freeland, H. (2001). Observations of the flow of abyssal water through the samoa passage. *Journal of Physical Oceanography*, *31*, 2273–2279.

Gamo, T. (1993). Philippine Sea abyssal waters in the northwestern Pacific: Characterization from tracer-tracer diagrams. *Elsevier Oceanography*, *59*, 91–104. https://doi.org/10.1016/S0422-9894(08)71320-5

Jackett, D. R., & McDougall, T. J. (1997). A neutral density variable for the world's oceans. *Journal of Physical Oceanography*, *27*, 237–263.

Johnson, G. C. (2008). Quantifying Antarctic bottom water and North Atlantic deep water volumes. *Journal of Geophysical Research*, *113*, C05027. https://doi.org/10.1029/2007JC004477

Kawabe, M., & Fujio, S. (2010). Pacific ocean circulation based on observation. *Journal of Oceanography*, *66*, 389–403.

Klocker, A., & McDougall, T. J. (2010). Influence of the Nonlinear Equation of State on Global Estimates of Dianeutral Advection and Diffusion. *Journal of Physical Oceanography*, *40*, 1690–1709. https://doi.org/10.1175/2010JPO4303.1

Ledwell, J. R., Montgomery, E. T., Polzin, K. L., St. Laurent, L. C., Schmitt, R. W., & Toole, J. M. (2000). Evidence for enhanced mixing over rough topography in the abyssal ocean. *Nature*, *403*, 179–182.

Mantyla, A. W., & Reid, J. L. (1983). Abyssal characteristics of the World Ocean waters. *Deep Sea Research, Part A*, *30*(8), 805–833.

Mantyla, A. W., & Reid, J. L. (1995). On the origins of deep and bottom waters of the Indian Ocean. *Journal of Geophysical Research*, *100*, 2417–2439.

Mashayek, A., Ferrari, R., Nikurashin, M., & Peltier, W. R. (2015). Influence of enhanced abyssal diapycnal mixing on stratification and the ocean overturning circulation. *Journal of Physical Oceanography*, *45*, 2580–2597.

McDougall, T. J., & Ferrari, R. (2017). Abyssal upwelling and downwelling driven by near-boundary mixing. *Journal of Physical Oceanography*, *47*, 261–283.

Moum, J. N., Perlin, A., Klymak, J. M., Levine, M. D., Boyd, T., & Kosro, P. M. (2004). Convectively driven mixing in the bottom boundary layer. *Journal of Physical Oceanography*, *34*, 2189–2202.

Polzin, K. L., Toole, J. M., Ledwell, J. R., & Schmitt, R. W. (1997). Spatial Variability of Turbulent Mixing in the Abyssal Ocean. *Science*, *276*, 93–96.

Roemmich, D., Hautala, S., & Rudnick, D. (1996). Northward abyssal transport through the Samoan passage and adjacent regions. *Journal of Geophysical Research*, *101*, 14039–14055. https://doi.org/10.1029/96JC00797.

Roussenov, V., Williams, R. G., Follows, M. J., & Key, R. M. (2004). Role of bottom water transport and diapycnic mixing in determining the radiocarbon distribution in the Pacific. *Journal of Geophysical Research*, *109*, C06015. https://doi.org/10.1029/2003JC002188

Thurnherr, A. M., & Speer, K. G. (2003). Boundary Mixing and Topographic Blocking on the Mid-Atlantic Ridge in the South Atlantic. *Journal of Physical Oceanography*, *33*, 848–862.

Troupin, C., Barth, A., Sirjacobs, D., Ouberdou, M., Brankart, J. M., Brasseur, P., et al. M. (2012). Generation of analysis and consistent error fields using the Data Interpolating Variational Analysis (Diva). *Ocean Modelling*, *52*, 90–101.

Voet, G., Girton, J. B., Alford, M. H., Carter, G. S., Klymak, J. M., & Mickett, J. B. (2015). Pathways, Volume Transport, and Mixing of Abyssal Water in the Samoan Passage. *Journal of Physical Oceanography*, *45*, 562–588. https://doi.org/10.1175/JPO-D-14-0096.1

Walin, G. (1982). On the relation between sea-surface heat flow and thermal circulation in the ocean. *Tellus*, *34*, 187–195.

Whitehead, J. A. (1998). Topographic control of oceanic flows in deep passages and straits. *Review of Geophysics*, *36*, 423–440.